DFT Calculations of Hydrogen Interactions with Pd and Pd/Ni Chain Functionalized Single-Walled Carbon Nanotubes for Sensor Applications

Ling Miao, Venkat R. Bhethanabotla and Babu Joseph
Department of Chemical Engineering, University of South Florida, Tampa, 33613 FL

Abstract

Density functional theory is employed to study Pd and Pd/Ni alloy monatomic axial and circular chain-functionalized metallic single walled carbon nanotube SWNT(6,6) and semi-conducting SWNT(10,0), and their interactions with hydrogen molecules. The stable geometries and binding energies have been determined for both isolated chains and chains on SWNT surface. We found that both axial and radial continuous Pd and Pd/Ni axial chains form on SWNTs with a geometry close to the stable geometry in the isolated chains. Ni alloying improves stability of the chains owing to a higher binding energy to both Pd and C atoms. The physical properties of SWNTs are significantly modified by axial chain-functionalization. SWNT(10,0) is transformed to metal by either Pd or alloy chains, as well as to a smaller gap semiconductor, depending on the Pd binding site. From calculations for H_2 interactions with the optimized axial chain SWNT systems, the adsorption energy per H atom is found to be about 2.6 times larger for Pd/Ni axial chain-functionalized SWNTs than for pure Pd chain-functionalized SWNTs. Band structure calculations show that the SWNT(10,0) reverts back to semi-conductor and SWNT(6,6) has reduced density of states at Fermi level upon H_2 adsorption. This result is consistent with the experimentally observed increase of electrical resistance when Pd coated SWNTs are used as H_2 sensing materials. Our results suggest that Pd/Ni-SWNT materials are potentially good H2 sensing materials. The behavior of H_2 interaction with circular chain-functionalized is currently being studied to compare with that of axial chain. Because of it discontinuity along the tube axis, the study of circular can be used to elucidate the major conduction path of Pd functionalized SWNTs, therefore it helps understand the sensing mechanism of electrochemical hydrogen senors based on conductivity change.

Introduction

Recently, modifications of single walled carbon nanotubes (SWNTs) have attracted much interest because they allow control of the properties of bare tubes (1, 2). A carbon nanotube with adsorbed metals can significantly change its physical properties, thereby providing a useful means for manipulating electron transport, which is of value in microelectronic device design (3). Our interest is in gas sensing materials. For example, Pd nanoparticle modified SWNT based sensors are shown to exhibit high sensitivity and fast response to hydrogen at room temperature (4, 5). Pd coated SWNTs have also shown some advantages over conventional sensors for methane detection, while bare SWNTs show no response to methane (6). It is expected that advanced gas sensors can be constructed from these metal functionalized carbon nanotubes. Thus, theoretical studies of interactions of metal atoms with SWNTs and their response to hydrogen gas are useful to understand and evaluate their potential for fabricating microelectronic gas sensor devices. The interaction of single metallic atoms with SWNTs has been systematically studied lately, using density functional theory (DFT) (7, 8). However, not much attention has been given to the continuous metal atom functionalized, especially metal alloy functionalized SWNTs (9, 10). Gas interactions with metal and alloy functionalized SWNTs have also received very little theoretical treatment so far. Such

studies have the potential of not only explaining sensors mechanisms but also of suggesting improved sensing materials. Issues such as the stability and structure of sensing material upon gas adsorption and nature of bonding can be addressed with DFT calculations using pseudopotential and plane wave methods. The pseudopotential approach is based on the discrimination between core and valence electrons. It considers the chemically inert core electrons together with the nuclei as rigid non-polarizable ionic cores, so that only the valence electrons have to be dealt with explicitly, and thereby significantly reduces the computational cost (11). The pseudopotential plane wave method for DFT calculations has been developed and perfected over many years into a reliable tool for predicting static and dynamic properties of molecules and solids (12). This method has been widely used in the theoretical calculations of SWNT systems, including functionalizations and interactions with gas molecules (13–15).

In this paper, we use DFT methods to study both pure Pd and Pd/Ni alloy monatomic chain-functionalized SWNTs and their interactions with H_2 molecules, because Pd is a well known element used in H_2 sensing materials (16–18). Prior research has shown the possibility of forming isolated single atomic chains (19–26). Electron beam evaporated Pd and Ni were shown to coat SWNTs with reasonable adhesion, indicating the possibility of experimentally realizing chain and cluster functionalized SWNTs with these metals (27). Therefore, a chain-functionalization study by DFT can be used to examine the stability of chain-SWNT materials as well as to demonstrate a higher adatom coverage, compared to single atom functionalization, thus better mimicking systems used in experiments. Ni is used as Pd-alloying element because, like Pd, Ni can also quickly adsorb H_2, hence is widely used in hydrogenation catalytic reactions (28). Moreover, Ni has been shown to be important for hydrogen sensors for improving reliability and speed of the sensor response in detecting hydrogen (29, 30). Theoretically, Ni is found to also have higher binding energy on SWNT than Pd (7). The effect of Ni on the performance of Pd functionalized CNTs is therefore of particular interest. In addition, we study another class of chain-functionalized SWNT systems, where Pd atoms are distributed discretely along the nanotube axis, but form continuously along the nanotube circumference.

In this work, we perform DFT calculations on both semiconducting SWNT(10,0) and metallic SWNT(6,6), with similar diameters of 7.83 Å and 8.14 Å. First, geometries and stability of free standing infinite Pd and Pd/Ni monatomic chains are analyzed. Then, Pd and Pd/Ni chains are constructed on the tube surface to examine the formation of chain-functionalized SWNTs. Finally, H_2 molecules are added to study the interactions and sensing mechanisms. Our primary goal is to reveal the character and geometries of Pd and Pd/Ni atomic chain-functionalized SWNTs and to understand the hydrogen interactions with these materials.

Method of Calculations

The Vienna *ab initio* simulation package (VASP) (31–34) was used to perform calculations within the generalized gradient approximation of PW91 (35) using optimized ultrasoft pseudopotentials (36, 37) and a plane wave basis set. The plane wave basis set assumes a supercell geometry that is periodic in all three directions. The single atomic chains and SWNTs were considered to be isolated and infinite in length, with lateral separation of more than 1 nm. The Brillouin zone of the supercell was sampled by Monkhorst-Pack special 1×1×31 k-points (38). Structural configurations

of isolated SWNTs were fully relaxed, and all atomic positions of adsorbate and adsorbing SWNTs were optimized until residual forces were within 0.05 eV/Å.

The binding energy E_b of chain atoms per unit cell can be calculated in terms of total energy of isolated atom and the chain formed by the same atoms, see Equation 1 and 2.

$$E_b^{(Pd\ chain)} = E_T^{(Pd\ chain)} - 2E_T^{(Pd)} \tag{1}$$

$$E_b^{(Pd/Ni\ chain)} = E_T^{(Pd/Ni\ chain)} - E_T^{(Pd)} - E_T^{(Ni)} \tag{2}$$

$$E_b^{(Pd\ chain+SWNT)} = E_T^{(Pd\ chain+SWNT)} - E_T^{(SWNT)} - 2E_T^{(Pd)} \tag{3}$$

Similarly, the binding energies of chain atoms per unit cell on SWNTs are calculated using Equation 3 and 4. E_T is the ground state total energy for the different fully-relaxed systems, and the factor 2 accounts for the number of Pd atoms in the unit cell. In all these calculations, there are two Pd atoms or one Pd and one Ni atoms per unit cell. Negative binding energies correspond to energetically bound species.

$$E_b^{(Pd/Ni\ chain+SWNT)} = E_T^{(Pd/Ni\ chain+SWNT)} - E_T^{(SWNT)} - E_T^{(Pd)} - E_T^{(Ni)} \tag{4}$$

Pd and Ni adsorbed SWNT systems have been reported as having a zero or very small magnetic moment (7, 39). Even so, we employed fully spin-polarized DFT calculations to observe any change in the magnetic moment of Pd and Pd/Ni chain-functionalized SWNTs.

Results and Discussion

Atomic Chain Structures

We first studied the Pd and Pd/Ni monatomic chain structures. Two configurations of chains were studied, namely, linear chain and zigzag chains. In the alloy chains, Pd and Ni atoms were located alternately. Results are shown in Figure 1, where the binding energy is plotted as a function of the chain unit cell length d in the chain direction. These curves show that Pd and Pd/Ni chains at local minima have larger-magnitude binding energies than in their own bulk systems, which is about -0.7 eV/bond for Pd face-centered cubic (fcc) bulk and -0.9 eV/bond for Ni fcc bulk, indicating the many atom effect in the bulk (24). The largest-magnitude binding energy of Pd linear chain is -1.21 eV/bond, close to the -1.20 eV/bond calculated by Bahn and Jacobsen (24). The binding energy of Pd/Ni linear chain at local minima is calculated to be larger in magnitude than that of the Pd linear chain, indicating a stonger binding of Pd-Ni than Pd-Pd.

We observe that zigzag chains have much stronger binding than the corresponding linear chains, which indicates that the preferred geometry of single atomic chain is not linear. The largest-magnitude binding energy of Pd zigzag chain can be found when Pd bonds form a narrow angle of 57.5º, with d=2.55 Å, corresponding to the Pd-Pd nearest neighbor (nn) distance of r_{nn}=2.55 Å, and Pd-Pd next near neighbor (nnn) distance of r_{nnn}=2.65 Å. The other meta stable state is located at d=4.00 Å, corresponding to the Pd-Pd nn distance of 2.45 Å and Pd-Pd nnn distance of 4.00 Å, with a wide bond angle of 109.1º. As seen in Figure 1, the Pd/Ni linear and zigzag chains have

3
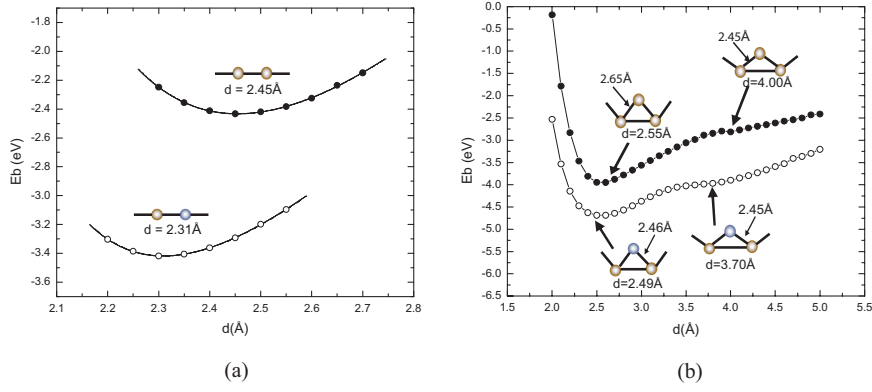
Figure 1: Calculated binding energy of Pd and Pd/Ni chain atoms per unit cell as function of length of unit cell d. Two geometries: (a) straight, (b) zigzag chains are shown as functions of d. The stable narrow angle and metastable wide angle zigzag chains are marked in the right figure. Black and white filled circles are for Pd and Pd/Ni chains, respectively. The binding energy is calculated from total energy difference between atomic chain and isolated atoms.

overall larger binding energies than those of pure Pd. The difference between the binding energies is about 0.25 eV smaller for the zigzag than for the linear chains. The first minimum for Pd/Ni zigzag chain appears at d=2.49 Å, which corresponds to the Pd-Pd and Ni-Ni distance of 2.49 Å, and Pd-Ni distance of 2.46 Å. The bond angle is 60.5º. The second local minimum appears for d=3.70 Å, corresponding to the Pd-Pd and Ni-Ni distance of 3.70 Å, and Pd-Ni distance of 2.45 Å, with a smaller bond angle of 98.1º.

Pure Pd Chain on SWNT

To form continuous chains on isolated SWNTs, each supercell contains two metal atoms along the tube direction. Due to different symmetries of (6,6) and (10,0) tubes, there are limited possibilities for placing chains on the SWNTs. Four sites were considered for Pd adsorption, as shown in Figure 2. Calculations of adsorption energies have shown that for the (6,6) tube, adsorption on bridge-1 site is the strongest, while for the (10,0) tube, the strongest adsorption site appears to be the bridge-2 site. From Figure 1, we see that the narrow angle chain is most stable and a wide angle chain is metastable. Based on this, we decided to add Pd wide angle chains on both bridge-1 and bridge-2 sites of the (10,0) tube and Pd narrow angle chains on top sites of (6,6) tube. The bond length and bond angle of the chains are slightly changed due to the curvature of the tubes. In the calculations, we did not observe magnetic moment in the Pd chain-SWNT systems.

The Pd chains maintain their overall initial geometries after relaxations. The angle between Pd atoms on (6,6) tube is 53.0º, with the nn distance of d=2.46 Å as in Figure 1. The curvature of the (6,6) tube and the stronger interactions of Pd-Pd atoms induce unequal Pd-C distance of 2.21 Å and 2.26 Å between the Pd atoms and their nearest carbon atoms. These distances are larger than the Pd-C distance of 2.10 Å formed by single Pd atom on the top site of the (6,6) tube. The bridge-1 site adsorbed Pd atoms on (10,0) tube form an angle of 107.7º with d=4.26 Å. This angle and distance d are close to those for the isolated wide angle chain, shown in Figure 1(109.1º and

4
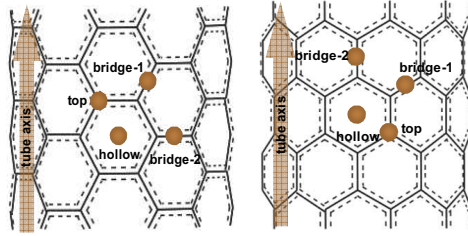
Figure 2: Schematic drawing of top views of four possible sites for single Pd atom adsorption on SWNT(6,6) and SWNT(10,0). Brown dots represent Pd atoms. Bridge-2 site differs from bridge-1 site in that the C-C bond is perpendicular to the tube axis at this site. In the SWNT(10,0) case, bridge-2 site is located on a C-C bond parallel to the tube axis.

4.0 Å). We also observed that the Pd adatoms rise above the bridge-1 site, with the Pd−C distance of 2.40 Å. For the (10,0) tube, the distances between the Pd atoms and their nearest C atoms are 2.13 Å and 2.12 Å, which are smaller than the 2.17 Å obtained for single Pd atom adsorbed on the bridge-1 site. The Pd chain on the bridge-2 site stabilizes at a bond angle 99.6° and $d = 4.27$ Å in its most energetically favorable geometry. Unlike bridge-1 site adsorption, both C atoms on bridge-2 sites of this (10,0) tube are only slightly further away (2.18 Å) from the carbon atoms than in the case of single Pd atom adsorption (2.14 Å). As also can be seen from cross sectional views in Figure 3, both types of SWNTs have slight radial distortions from circular shape to an elliptical shape with major and minor axes of R_1 and R_2, respectivly. We calculated radial strain parameters using Equation 5 and 6 defined in terms of magnitude of changes for the tubes.

$$\epsilon_{R_1} = \frac{R_1 - R_{0_1}}{R_{0_1}} \tag{5}$$

$$\epsilon_{R_2} = \frac{R_2 - R_{0_2}}{R_{0_2}} \tag{6}$$

R_0 is radius of the undeformed (zero-strain) nanotube in the absence of Pd. It is found that the Pd chain introduces tensional strain along R_1 and compressional strain along R_2. The Pd wide angle chains on the two different bridge sites of SWNT(10,0) introduce a different radial strain with bridge-1 site producing a much larger tensional strain (for which, $\epsilon_{R_1}=+0.052$) and compressional strain ($\epsilon_{R_2}=-0.020$) than bridge-2 site (ϵ_{R_1} and ϵ_{R_1} are +0.027 and −0.003, respectively). The Pd narrow angle chain has a negligible effect on SWNT(6,6) with $\epsilon_{R_1}=6.5\times10^{-4}$ and $\epsilon_{R_2}=0$.

The calculated binding energies per unit cell for the chain atoms on SWNT(6,6) and SWNT (10,0) are listed in Table 1. The adsorption energies for the single Pd atom on four different sites range from ∼−1.20 eV to ∼−1.50 eV, and the average Pd-tube distance length is in the range of 2.10-2.18 Å (40). In this case of Pd chain formation on carbon nanotube, due to the strong Pd-Pd binding in the chain, the binding energy per Pd atom is ∼−1.88 eV to ∼−2.00 eV, much larger in magnitude than that of the single atom adsorption. These values are compared with the binding energy of Ti chain on SWNTs, reported as ∼−3.24 eV to ∼−4.08 eV (9). Ti shows stronger binding with SWNTs than many other metals, and can form continous wires. From results of this work, we conclude that Pd/Ni chain formation on SWNTs is energetically favored. The Pd atoms have larger
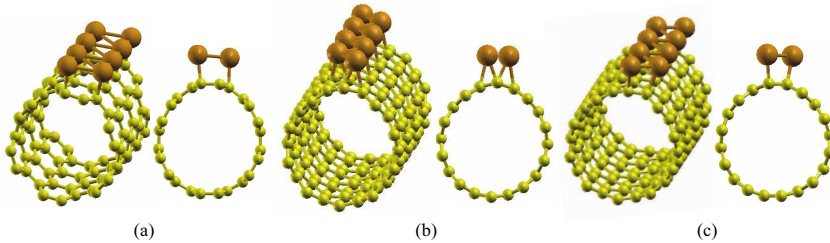
Figure 3: 3D view of equilibrium geometries of the Pd chain SWNT structures. (a) Pd narrow angle chain on top site of SWNT(6,6), (b) Pd wide angle chain on bridge-1 site of SWNT(10,0), (c) Pd wide angle chain on bridge-2 sites of SWNT(10,0). In all cases, changes in the tube shape are seen from the cross sectional views.

Table 1: Binding energy of Pd atoms per unit cell on two SWNTs. d_{Pd-C} is the distance between Pd and its nearest neighbor C atom. ΔQ is the electron charge transfer from tube to adatoms, where positive represents charge transfer to tube.

System	E_b(eV)	d_{Pd-C}(Å)	d_{Pd-C}(Å)	ΔQ(e)
Pd chain + SWNT(6,6)	−4.01	2.26	2.21	0.11
Pd chain + SWNT(10,0)[†]	−3.75	2.13	2.12	0.20
Pd chain + SWNT(10,0)[‡]	−3.81	2.18	2.18	0.22

[†] Values measured on bridge-1.

[‡] Values measured on bridge-2.

binding energy on the (6,6) tube than on the (10,0) tube partially because of the stronger binding of Pd atoms in the narrow angle geometry. Comparing the two studied wide angle chains of similar geometry on bridge-1 and bridge-2 sites on the (10,0) tube, we see that although bridge-1 site chain is closer in geometry to the meta-stable isolated chain structure, the larger-magnitude binding energy appears for bridge-2 site binding. We attribute this to the larger-magnitude adsorption energy of Pd atom on bridge-2 site than on bridge-1 site of (10,0) tube as seen in our recent calculations (40).

The electronic structures of the bare as well as Pd chain decorated SWNTs for both the (6,6) and (10,0) tubes are presented in Figure 4 and 5, respectively. Figure 4(a) shows the band structure and electron density of state of a (6,6) tube. The conduction band and valence band meet at Fermi level indicating that the tube is metallic. The separation between two van Hove singularities around Fermi level is 3.65 eV, which is in agreement with results of Reich *et al.* (41). Figure 5a shows the band structure and DOS of the semiconducting (10,0) tube. The band gap between the bottom of the conduction band and top of the valence band at Γ point is about 0.75 eV, also in agreement with previous results (42).

Figure 4(b), 5(b), and 5(c) show that upon adsorption of Pd chains, the electronic properties of both SWNTs undergo many significant changes. The originally degenerated states are split in both valance and conduction bands due to symmetry breaking of the wave function. As shown in Figure 4(b), the Pd-SWNT(6,6) system remains metallic. In fact, an increase in density of states
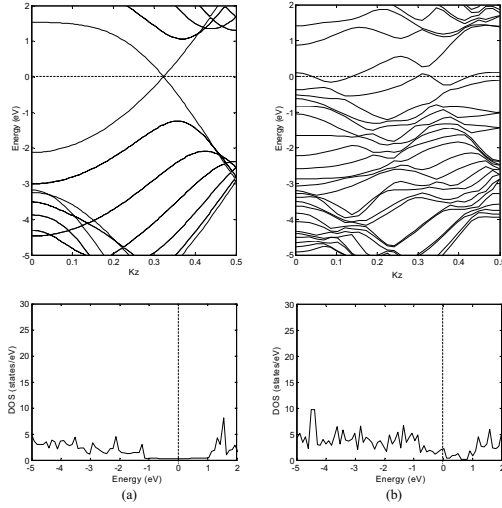
Figure 4: Spin-polarized band structure and DOS of (a) SWNT(6,6) and (b) Pd narrow angle chain adsorbed SWNT(6,6). Fermi level is set as zero.
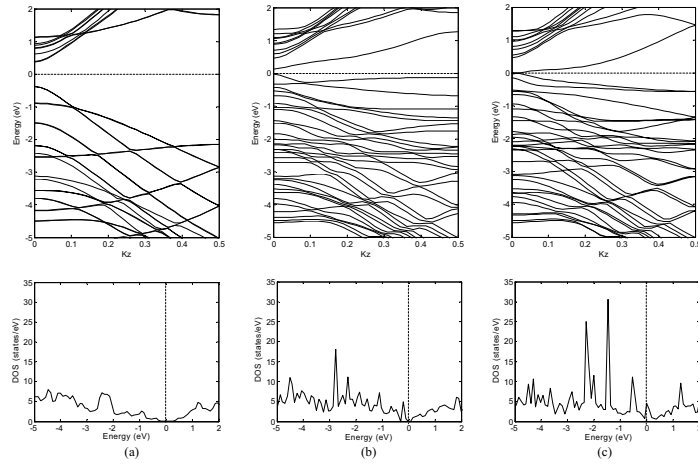
Figure 5: Spin-polarized band structure and DOS of (a) SWNT(10,0), (b) Pd wide angle chain adsorbed on the bridge-1 sites of SWNT(10,0), and (c) Pd wide angle chain adsorbed on the bridge-2 site of SWNT(10,0). Fermi level is set as zero.

around Fermi level leads to a higher electrical conductivity of the Pd-SWNT(6,6) system. The charge transfer study (43) shows there is about 0.1 eV per unit cell electron transferred from Pd chain to the (6,6) tube. As shown in Figure 5(b) and 5(c), the band structures of (10,0) tube show different electrical property changes upon the adsorption of Pd chains on different sites. In the bridge-1 site adsorption, band gap of the bare tube is significantly reduced to a low 0.15 eV. The existence of this small gap suggests that the system is a narrow gap semiconductor material. However, when Pd chain is added on the bridge-2 sites, metallic character is observed through crossing of the Fermi level near Γ point, with DOS at the Fermi level of 4.5 states/eV. Approximately 0.20 and 0.22 electrons transfer from bridge-1 and bridge-2 site Pd chains to the (10,0) tubes, respectivly. All this suggests that different electronic properties of a carbon nanotube can be achieved through decorations of the tube by the same element on different sites.

Pd/Ni Alloy Chain on SWNT

Pd/Ni alloy chain-functionalized on the same tubes were studied by substituting alternate Pd atoms with Ni atoms, and then relaxing the systems. Ni atom is reported to have stronger binding with semiconducting tube (8,0) than Pd atom (7), and Ni can also improve the reliability of Pd nanomaterials, especially in hydrogen sensing applications (29, 30). Here, we used the same initial configurations as the pure Pd chains functionalized SWNT systems, however we found the total energy was not converging during relaxation of the bridge-1 site adsorbed Pd/Ni chain+SWNT(10,0) system. Therefore, in the study of Pd/Ni alloy chains on SWNTs, we considered only two configurations, namely the narrow angle alloy chain on top site of SWNT(6,6) and wide angle chain on bridge-2 site of SWNT(10,0). Their equilibrium geometries are shown in Figure 6. Significant changes in the cross sectional shape of tubes are observed as shown in Figure 6(b). SWNT(6,6) mostly retains its circular cross sectional geometry because of the weakened Pd-C interactions induced by strong Pd-Ni coupling. Again, radial strain calculation shows a negligible strain effect introduced by Pd/Ni narrow angle chain on SWNT(6,6). However the Pd/Ni wide angle chain produces +0.056 tensional strain along R_1 and −0.037 compressional strain along R_2 of SWNT(10,0), which are both much larger than for the pure Pd wide angle chain on the same site shown in Figure 3(c). A larger binding energy was observed than in the case of pure Pd atoms on the same tubes, as shown in Table 2. In both cases, we observed a much smaller distance between Ni and C atoms than between Pd and C atoms. The bond angles of Pd/Ni chain on (6,6) tube and (10,0) tube are 57.5º and 112.3º, respectively, very close to the angles of 60.5º and 98.1º in their stable geometries as isolated chains, as shown in Figure 1.

The spin polarized band structures shown in Figure 7 are similar in form to the ones obtained for SWNT(6,6) and SWNT(10,0) decorated with Pd chains, cf. Figure 4 and 5. However, we now observe splitting of the spin bands, more so in the case of Pd/Ni chain adsorbed SWNT(6,6) than in case of Pd/Ni adsorbed SWNT(10,0). We therefore conclude that the introduction of Ni atoms produces magnetic moment in the systems, higher in the case of metallic SWNT(6,6). Table 2 lists corresponding values for μ.

The additional bands in the band gap region are related to the delocalized states from the Pd/Ni chain. For instance, from the atom projected DOS in Figure 8, we can clearly see that they are contributed by the states from both Ni and Pd, and the neighboring C atoms. The major binding state
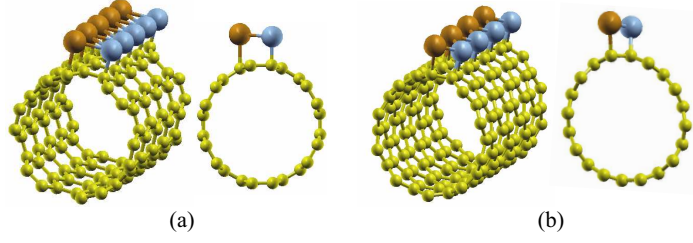
Figure 6: 3D views of equilibrium geometries of the Pd/Ni chain-tube structures. (a) Pd/Ni narrow angle chain on top site of SWNT(6,6), (b) Pd/Ni wide angle chain on bridge-2 site of SWNT(10,0).

Table 2: Calculated binding energies, charge transfer, and magnetic moment for Pd/Ni chain-SWNT system. d_{Pd-C} is the distance between Pd and its nearest neighbor carbon atom. d_{Ni-C} is the distance between Ni and its nearest neighbor carbon atom. ΔQ is the electron charge transfer from tube to adatoms, where positive value means tube gains charge.

System	E_b (eV)	d_{Pd-C} (Å)	d_{Ni-C} (Å)	ΔQ(e)	$\mu(\mu_B)$
Pd/Ni chain + SWNT(6,6)	-4.98	2.36	1.97	0.18	0.76
Pd/Ni chain + SWNT(10,0)[†]	-4.34	2.24	1.99	0.30	0.08

[†] Values measured on bridge-2.
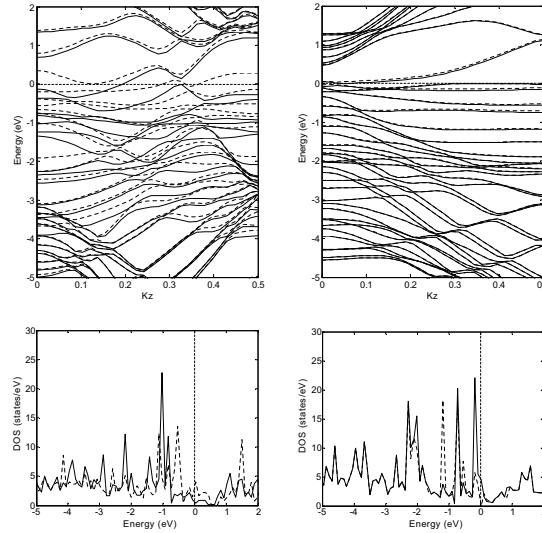
Figure 7: Spin-polarized band structure and DOS of (a) Pd/Ni narrow angle chain functionalized SWNT(6,6), and (b) Pd/Ni wide angle chain functionalized SWNT(10,0). Fermi level is set as zero.

9
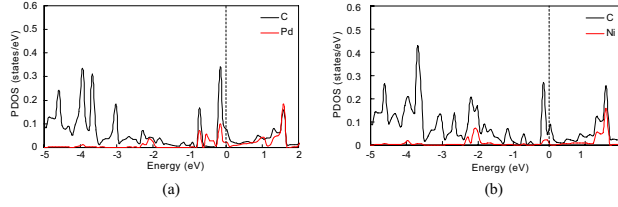
Figure 8: Atom projected density of state (PDOS) from (a) Pd atom with two nearest C atoms and (b) Ni atom with two nearest C atoms, on bridge-2 site functionalized SWNT(10,0).
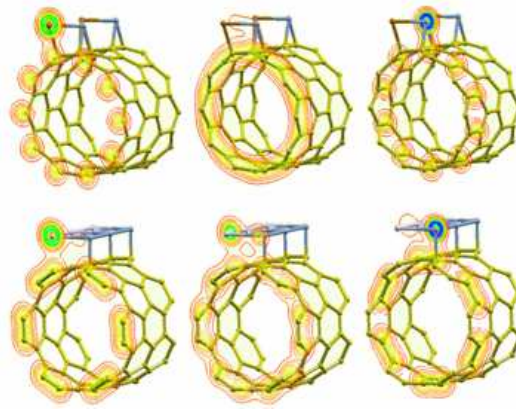
Figure 9: Contour plot of total (spin-up and spin-down) valence charge density on three planes for Pd/Ni chain functionalized SWNT(10,0) (upper) and Pd/Ni chain functionalized SWNT(6,6) (lower). The planes are through the cross section of the tube and different location on the Pd/Ni chain.

of Pd and Ni with their nearest C atoms appears at about -0.75 eV and -2.00 eV, respectively. This suggests a stronger binding between Ni and C than between Pd and C. To further explore the electronic interactions and delocalization of electrons belonging to Pd, Ni and SWNT, we have plotted the total electron density across various cross-sections of the Pd/Ni chain functionalized SWNTs in Figure 9. As shown in Figure 9, electrons in the area under chains are delocalized and distribute on both metal and carbon atoms. The charge transfer shown in Table 2 indicates that a larger number of electrons were transferred upon alloying, more onto the SWNT(10,0) than onto the SWNT(6,6). The magnetization density, defined as the difference between spin up and spin down density, shown in Figure 10 shows that a strong positive magnetization density located on Ni atom, indicating the magnetic moment is mostly carried by Ni, but not by Pd or tubes. Comparing the two tube systems, we notice that no magnetization density is found at SWNT(10,0) C atoms, but a low magnetization is found distributed on the C atoms on the SWNT(6,6), showing the de-localization of the magnetic moment. The distribution of the magnetization density around the Ni atom resembles different shapes in two chain-SWNT systems: a d-like orbital shape on (10,0) tube and a p-like orbital shape on (6,6) tube.

H_2 Interactions with Chain-Functionalized SWNTs

10
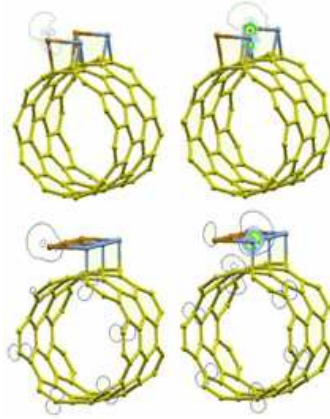
Figure 10: Contour plot of magnetization density (spin-up and spin-down) on two planes through Pd or Ni and the tube for the same systems as in Figure 9.

Experimentally, Pd functionalized SWNT have been studied as H_2 sensors, and good response have been observed through a large change in resistance (5). Theoretical (44, 45) and experimental (46, 47), studies have shown that molecular hydrogen interaction with bare carbon nanotubes is a weak physisorption process, with low adsorption energy. The chemisorption state with molecule dissociation has been found as hydrogen molecule is very close to the tube surface, however approximate energy barriers of 2.5 eV (48, 49) and 3.4 eV (50) are needed to be overcome for SWNT(6,6) and (10,0), respectively, to dissociatively chemisorb a H_2 molecule onto the tube. In this section, we study the interactions between H_2 molecules and functionalized SWNTs by placing one H_2 molecule on top of both Pd and Ni atoms. We have tried two different ways of placing H_2 molecules by letting H-H bond either parallel or perpendicular to chain-SWNT axis. After relaxing the systems, we did not observe any significant differences in final geometry or binding energy. The results shown here are from the initial structures where H-H bonds are parallel to the tube axis as shown in Figure 11. For a comparison of the different interactions between pure Pd chain and Pd/Ni alloy chain functionalized SWNTs, we study four out of five systems shown in Figure 3 and 6, except for the bridge-1 site Pd functionalized SWNT(10,0).

The dihydrogen complex of H_2 and Pd was reported to have an H-H bond length of 0.86 Å, and a Pd-H bond length of 1.67 Å (51). Our calculation of a free PdH_2 gave the same result. In investigating the adsorption of a H_2 molecule on Pd and Pd/Ni chain functionalized SWNT(6,6) and SWNT(10,0), we observed the dissociation of H_2. The distance between the two dissociated H atoms is 0.83 Å on Pd and 0.86 Å on Ni on both types of carbon nanotubes, therefore we conclude that the final geometry of individual H_2 molecule on Pd is not affected by the species of its neighbor atoms. We have calculated the adsorption energy of one H atom with respect to the H_2 molecule according to Equation 7.

$$E_{ad}^{(H)} = -\frac{1}{4}\left[E_T^{(chain+SWNT+4H)} - E_T^{(chain+SWNT)} - 2E_T^{(H_2)}\right] \tag{7}$$

We obtained the binding energies of -0.13 eV and -0.33 eV for pure Pd functionalized SWNT(6,6) and SWNT(10,0),respectively, and -0.17 eV and -0.48 eV for the same alloy functionalized systems. The negative values of these binding energies could be compared with the adsorption energy per H
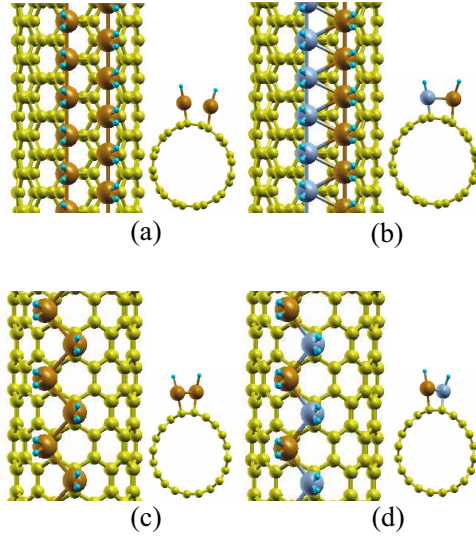
Figure 11: 3D views of equilibrium geometries of the H_2 adsorbed Pd and Pd/Ni functionalized SWNTs. The color scheme is same as previous figures. Small bright blue dots are hydrogen atoms. (a) and (b) are SWNT(6,6) systems, (c) and (d) are SWNT(10,0) systems.

atom(energy gain per H atom upon adsorption of a H_2 molecule on the surface) at low to medium hydrogen coverage ($\Theta<1$) on Pd single crystal surfaces of 0.45~0.5 eV. (52, 53) Differences between our calculated values for the Pd-SWNT cases and the literature values for the Pd surfaces are from the differences in the surface coordination of adsorption sites in these different systems. Stronger adsorption is seen in the alloy functionalized systems. The adsorption energy decreases strongly with increasing hydrogen coverage. (53, 54) For example, at $\Theta=1.25$, the adsorption energy can be as low as about half of the adsorption energy at $\Theta=1$. Our results show that a Pd narrow angle chain functionalized SWNT(6,6) has much lower H_2 adsorption energy than a Pd wide angle chain functionalized SWNT(10,0). This is mainly because of the higher Pd local density of the narrow angle chain, which provides less open space for H_2 adsorption. We also find that Ni alloyed Pd chain functionalized tubes have higher H_2 adsorption energy compared to the pure Pd functionalized tubes. This seems to conflict with the fact that Ni-alloying decreases H_2 sensitivity in sensor application. However, an alloying induced sensitivity decrease is usually seen in the experiments where film thickness is from about 50 to about 2000 nm. In that case, a H_2 diffusional transport is mainly responsible for the sensitivity, in other words, the magnitude of the response. Since the diffusion coefficient for H atoms in Pd is about 10^2 times larger than in Ni at room temperature (55), we usually see a decreased sensitivity of hydrogen sensors when Pd is replaced by Ni. If the hydrogen diffusion process is not a limitation, such as when an atomically thin film is used, then we would see a better H_2 sensitivity on Ni, as Ni has a higher H_2 adsorption energy than Pd (52, 56, 57). This is also why we see larger adsorption energy when Pd/Ni alloy chains are decorated on both types of SWNTs.

Adsorption of H_2 molecules changes the geometry of chains on the tubes in two aspects, as shown in Figure 11: the bond angle of metal chains and the distance between metal atoms and carbon atoms. From the calculations, we have seen the overall bond angles of atomic chains decrease with

12
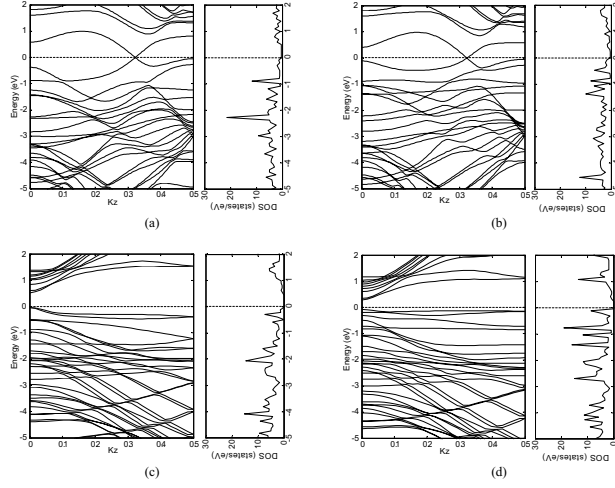
Figure 12: Band structure and DOS for the four systems shown in Figure 11.

an almost unvaried d. For example, the bond angle of pure Pd chain on SWNT(6,6) and (10,0) decrease to 49.3º and 97.6º from 53.0º and 99.6º, and alloy chains decrease to 52.8º and 106.0º from 57.5º and 112.3º. Upon H_2 adsorption, the Pd chain on SWNT(6,6) shows a large expansion, nearly separating the zigzag chain into linear chains. Other systems also have shown different degrees of chain expansion toward two different directions. This is mainly caused by the H repulsion, which is larger on narrow angle chains. On the other hand, we find the introduction of H_2 molecules strengthens the metal-carbon binding by lowering the chains on the tube surface. We have observed that with H_2, Pd−C distances from pure Pd wide angle chain-SWNT(10,0) system increase about 1.7%, but the Pd−C and Ni−C distances from Pd/Ni chain on the same (10,0) tube show no length change. In the narrow angle chain−SWNT(6,6) systems, due to the significant change of the chain geometry, Pd-C distances have a slight decrease of 0.6% compared to chain-SWNT(6,6) without H_2, while Pd-C and Ni-C distances in alloy chain decrease about 3.1% and 2.2%, respectively after H_2 is adsorbed on the (6,6) tube. These observations indicate that the presence of H_2 affects the chain geometry and adatom binding with SWNT differently. For different systems, large morphology changes are observed in narrow angle chain-tube systems. A strong Ni-Pd binding from Ni alloying prevents narrow angle chain from splitting and peeling from tube surface upon exposure to H_2. As for the carbon nanotube geometry, from Figure 11 and axial strain parameter calculations, we find that H_2 produces less strain to functionalized (10,0) tubes, where the initial distortion by Pd and Pd/Ni functionalization shown are maintained. The largest H_2 induced tube geometry change is observed on pure Pd chain functionalized (6,6) tube due to the chain splitting, where tensional strain along R_1 is +0.025 and compressional strain along R_2 is −0.033.

In Figure 12, we present the band structure and DOS for the four systems. We note that the adsorption of hydrogen changes the electronic properties of chain functionalized SWNTs. The electron density of states of the (6,6) tubes around Fermi level (Fig. 12(a) and 12(b)) decreases significantly compared to the DOS of Pd-chain-SWNT(6,6) (Fig. 4(b)) and of Pd/Ni-chain-SWNT(6,6) (Fig. 7(a)). In Figure 12(c) and 12(d), we see the band gap of 0.58 eV and 0.35 eV at Fermi level in Pd and Pd/Ni chain functionalized (10,0) tubes, indicating the systems are transformed back from metal to semiconductor. Both the decrease of electron density of states in the SWNT(6,6)

13

systems and the band gap opening in the SWNT(10,0) systems imply a significant increase of electrical resistance of the material. This result is consistent with experimental observations from other groups, where Pd coated SWNTs have been utilized in H_2 sensing (4, 5). In these experiments, an individual Pd coated semiconducting SWNT (4) and a Pd coated thin, uniform SWNT film (5) were used, respectively. Both experimental results show dramatic, reversible increase of resistance of the sensing materials upon exposure to hydrogen gas flow, indicating Pd coated SWNTs have very good sensitivity for H_2 detection. The single tube sensor configuration utilized by Kong *et al.* (4) consists of discrete Pd particles decorating the tube surface, while the random matrix of surface-dispersed SWNTs (5) were connected with a more or less continuous Pd film. In comparison, our calculations are for a continuous monatomic wire on the SWNT. Both the literature reported experimental results and our DFT calculations show that the resistance increases upon H_2 exposure. If we construct a series-parallel array of resistances composed of metal and SWNT segments as an equivalent circuit, then our DFT calculations can be interpreted to indicate that both continuous coating by metal and decoration by discrete particles of both metallic and semi-conducting SWNTs lead to the same response of increased resistance in hydrogen sensor applications. However, the magnitudes of response depend on the nature of the tube, being larger for semi-conducting SWNTs.

Charge transfer upon H_2 adsorption would indicate whether the resistance change is primarily in the tube or coating. Our analysis shows that H atoms are slightly negatively charged and the originally negatively charged SWNTs gain more charge. Pd and Pd/Ni functionalized SWNT(6,6) both gain 0.14 e, and SWNTs(10,0) gain 0.03 e and 0.06 e, respectively. Thus, upon H_2 adsorption, the two functionalized SWNT(6,6) gain about 0.1 e more charge than the two functionalized SWNT(10,0). Pd/Ni chains do not bring significantly larger amount of charge transfer to both types of SWNTs than Pd chains. The extra charge transfer from chains to SWNTs is due to the H_2 adsorption, which readjusts the positions of Pd and Ni atoms on the tube surface and cause charge redistributions between chains and SWNTs. This is especially true for the SWNT(6,6), where the narrow angle geometry yields a large chain expansion or splitting after adsorbing H and induces a significant charge redistribution. These charge transfer results suggest that H_2 sorption brings more electrons to the initially negatively charged SWNT from the chain functionalization. While this may indicate a decrease in tube resistance, the overall system resistance is indicated to increase from the band structure and DOS results. Hydrogenating of the metal appears to increase resistance significantly. Finally, we note that after H_2 adsorption, the initial magnetic moment carried by the Pd/Ni systems disappear and the systems turn nonmagnetic. The demagnetization of Ni bulk and surface by H_2 adsorption were understood as the involvement of the Ni *d*-states with H *s*-state, which tends to make *d*-shell more nearly full and as a consequence considerably reduces the magnetic moment (58, 59).

H$_2$ Interactions with Radial Chain-Functionalized SWNTs

In order to construct an axially noncontinuous Pd chain-functionalized SWNT system, the Pd monatomic chain, containing 20 Pd atoms per supercell, is placed around carbon nanotube on bridge-2 sites, as shown in Figure 13. Two carbon nanotube primitive unit cells containing 80 C atoms are used in each supercell. Each radial chain is separated of about 8 Åon the SWNT surface, therefore is considered noncontinuous along nanotube axis. In this chapter, only semiconducting SWNT(10,0) is studied. (According to our previous study, Pd chain-functionalized SWNT(6,6)
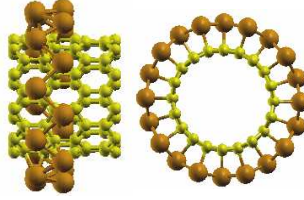
Figure 13: Equilibrium geometries of Pd radial chain-functionalized SWNT(10,0).
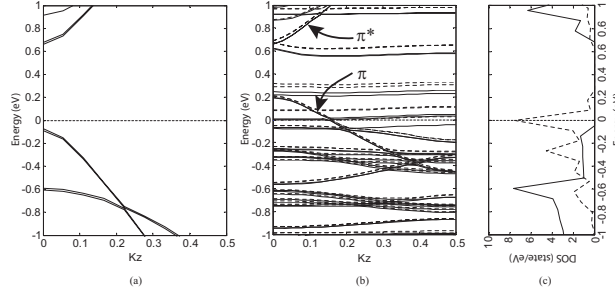
Figure 14: Spin-polarized band structure of (a) bare SWNT(10,0) and (b) Pd radial chain-functionalized SWNT(10,0). (c) The density of states of C atoms in a bare SWNT(10,0) and functionalized SWNT(10,0) are shown as solid and dotted line, respectively . Fermi level is set at 0 eV (horizontal dotted line).

show similar behavior as chain-functionalized SWNT(10,0).) Semiconducting carbon nanotubes are more commonly used in conductivity based hydrogen sensors rather than metallic carbon nanotubes (4, 48, 60).

The calculated electronic band structures near Fermi level are presented in Figure 14(a) and (b). A bare SWNT(10,0) is a semiconductor having a band gap of 0.75 eV. Pd radial chain increases the Fermi energy and yield additional flat spin-up and spin-down bands in the band gap of the bare SWNT. This agrees with the calculated magnetic moment of 1.2 μB of the system. The SWNT(10,0) is metallized upon on Pd adsorption in the form of a radial chain because the bands cross the Fermi level due to increase of Fermi energy and the hybridization between C p states and Pd d states. The original gap between the SWNT(10,0) binding (π) and anti-binding (π^*) bands reduce to $\sim$0.45 eV. The summation of DOS of 80 C atoms in Figure 14(c) exhibiting high density at Fermi level, implies such a transform is contributed by the carbon nanotube. Charge transfer analysis shows a total of 2.1 electrons were transferred from Pd to the SWNT, which is accordance with the band structure and DOS results.

The binding energy per Pd atom per super cell, calculated from Equation 8, is -1.9 eV. This indicates Pd atoms in radial chain-functionalized SWNT have stronger binding energy than that of a single Pd functionalized SWNT, which is known to be -1.5eV from previous calculations. We note that this value of -1.9 eV is almost same as the binding energy of Pd in a axial chain-functionalized SWNT, implying the chain geometry has negligible effect on binding energy when the Pd are placed
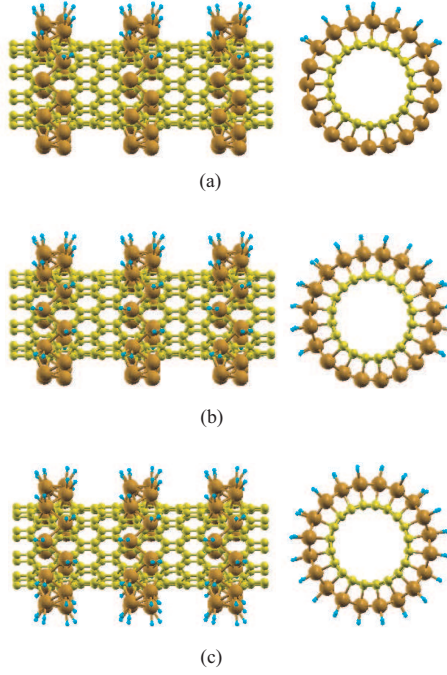
Figure 15: 3D views of equilibrium geometries of hydrogen adsorbed Pd radial chain-functionalized SWNT(10,0). From top to bottom: Θ=0.35, 0.60, 1.00.

in the same sites, such as the bridge-2 site in this case.

$$E_b^{(Pd)} = \frac{1}{N}\left[E_T^{(SWNT+NPd)} - E_T^{(SWNT)} - NE_T^{(Pd)}\right], N = 20 \tag{8}$$

A shorter average nn Pd-C distance of 2.13 Å is observed in the radial chain-SWNT, compared to the corresponding distance in the axial chain-SWNT. However, the average nnn Pd-C distance increases, namely each Pd atom is no longer equally bounded by the two bridge-2 C atoms as it is in the axial chain. The average angle between Pd atoms is 88.6°, with the average nn and nnn Pd-Pd distance of 2.72 Å and 3.83 Å. The decreases of nn and nnn distance and chain angle compared to the SWNT supported axial chain can be attributed to the curvature of the chain induced by the SWNT. From the cross sectional view in Figure 13, the tube does not appear to be distorted as shown in Figure 3, where an elliptical shape with a major axis under Pd chain is seen. The measurement of radial distance along the circumference of the SWNT indicates the adsorption of Pd atoms slightly expands the tube diameter, where Pd radial chain is placed, by ∼1%, while the diameter of the cross section not adsorbed by Pd chain is not affected.

Next we study the H_2 interactions with Pd radial chain-functionalized SWNT. Different hydrogen coverages, Θ, (Θ is calculated by the ratio of the number of H_2 molecules to Pd atoms) of 35%, 60% and 100%, are used. Their equilibrated structures are illustrated in Figure 15.

The adsorption energy of one H atom with respect to H_2 molecule is calculated by Equation 9.

Table 3: H$_2$ adsorption energies E_{ad}, averaged atomic distances $\bar{d}$, averaged nearest neighbor distances $\bar{n}n$, chain angles $\bar{\alpha}$, and magnetic moment μ for Pd radial chain-functionalized SWNT(10,0) systems with different H$_2$ coverage. $\bar{d}$, $\bar{n}n$ and $\bar{\alpha}$ are measured for H adsorbed Pd atoms only. The results are averaged over the number of adsorbed H$_2$ molecules.

Θ	E_{ad} (eV)	$\bar{d}_{H-H}$†	$\bar{d}_{Pd-H}$†	$\bar{n}n_{Pd-C}$†	$\bar{n}n_{Pd-Pd}$†	$\bar{\alpha}$‡	μ (μB)
0.00	–	–	–	2.13	2.72	89.3	1.22
0.35	0.38	0.84	1.76	2.15	2.79	88.5	0.96
0.60	0.37	0.84	1.77	2.15	2.78	86.1	–
1.00	0.37	0.84	1.77	2.15	2.79	86.3	0.00

† Values reported in angstrom.

‡ Values reported in degree.

$$E_{ad} = -\frac{1}{N}\left[E_T^{(SWNT+chain+NH)} - E_T^{(SWNT+chain)} - \frac{N}{2}E_T^{(H_2)}\right] \tag{9}$$

where N is the total number of H atoms. The results of H adsorption energy are shown in Table 3. Comparing with the axial chain-functionalized SWNT, H$_2$ has higher dissociative adsorption energy on the radial chain-functionalized SWNT. This can be contributed to the fact that the radial chain geometry has a smaller surface relaxation upon H$_2$ adsorption. This is seen from the comparison of axial and radial chain structure change before and after H$_2$ adsorption. Table 3 indicates that the distance between two dissociated H atoms and Pd-H bond length are not affected by the coverage, because every H$_2$ is adsorbed on different Pd atoms.

For partially adsorbed H$_2$ on radial chain-functionalized tubes (Θ=0.35, Θ=0.60), the nn distance of Pd radial chain in the part that is covered by hydrogen is larger than the part that is not covered, which is about the same as $\bar{n}n_{Pd-Pd}$ at Θ= 0. At the Θ=1.00, the nn of the Pd radial chain is larger than that of the unabsorbed Pd radial chain-functionalized tube. This is most likely caused by the repulsion of H atoms as also seen in the previous chapter of axial chain-functionalized tubes. Due to the adsorption of H$_2$ molecules, Pd atoms show a slight displacement on the SWNT(10,0), however the Pd-C nn distances increase less than 1.0% with respect to the corresponding distances before H$_2$ adsorption. This observation is different from the axial chain-functionalized SWNT(10,0), where a larger increase of 1.7% of Pd-C distances was seen upon H$_2$ adsorption. Pd atoms in the radial chain have less freedom of motion than in the one dimensional axial chain on the SWNT, and this prevents these Pd atoms from moving on H$_2$ adsorption.

Unlike Pd axial chain-functionalized SWNT(10,0), Pd radial chain-functionalized tube has magnetic moment of 1.22 μB. The onset of magnetism is associated with the increase of density of states at Fermi level, caused by the local symmetry change, or by the increasing the percentage of Pd atoms, as discussed by Sampedro et al. (61). The magnetic moment carried by the system decreases as the hydrogen coverage increases, as a results of the filled-up 4d states and the consequent reduction of density of states at Fermi level (62). Charge density calculations show 0.005 electrons per H atom are transferred from Pd to H atoms. The electron density associated with the Pd functionalized SWNT increases by ~0.2 eV at Θ=1.
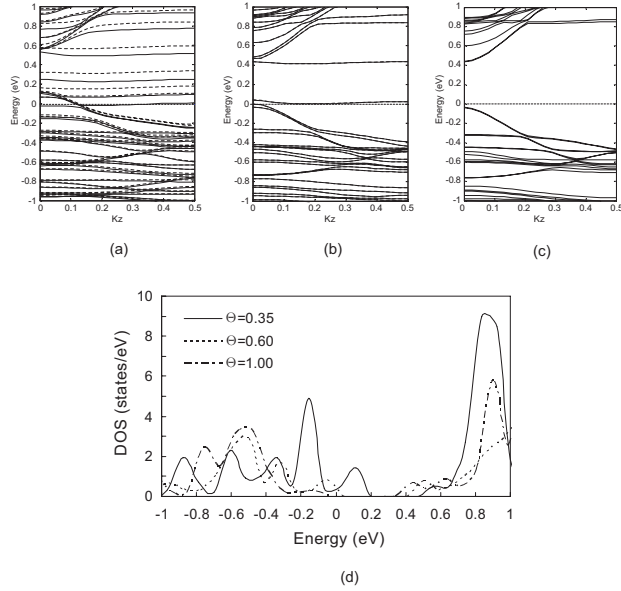
Figure 16: Spin-polarized band structure of hydrogen adsorbed on Pd radial chain-functionalized SWNT(10,0). From (a) to (c): Θ=0.35, 0.60, 1.00. (d) Local DOS of Pd atoms at different Θ.

According to the band structure, the hydrogen-induced band appears $\sim$8 eV below Fermi level of the Pd-SWNT system, in agreement with the value reported in the Pd-H system (63, 64). Due to the presence of H atoms in the Pd, the Fermi energy is shifted upward relative to the d band of Pd. Prior to H_2 adsorption, the Pd d band is mostly filled. The adsorption of H atoms drastically reduces the DOS at the Fermi level with a corresponding decrease in the number of anti-bonding bands near Fermi level as shown in Figure 16(a) and (b). At high H coverage, the d band becomes completely occupied, resulting in a zero DOS at Fermi level. As a consequence, the band gap from the SWNT reappears at Fermi level. The gradual decrease of DOS of Pd atoms with increasing Θ can be clearly seen from the summation of local DOS of each Pd atom in Figure 16(d). The band structure and DOS change of Pd due to Pd hydride formation upon hydrogen adsorption has been discussed by Chan and Louie (65). As shown in Figure 16(a)-(c), the metallic nature is maintained at Θ=0.35, 0.60, and band gap of $\sim$0.48 eV appears at Θ=1.00, indicating that the metallic Pd radial chain-functionalized SWNT has been transformed to a semiconductor. The resulting band gap is about the same size as the π-π^* gap of Pd functionalized SWNT before H_2 adsorption as shown in Figure 14(b), consistent with the charge preservation of the tube during H_2 adsorption. The reappearance of the band gap would imply a significant response in the sensor application. Since it is clear that the Pd atoms are discrete along the tube direction, our DFT calculations can be interpreted to indicate that both continuous and noncontinuous decorations by Pd of SWNT(10,0) lead to the same response of increased resistance in hydrogen sensor applications. This is in agreement with experimental observations of Kong *et al.* (4) and Sippel-Oakley *et al.* (5), where a noncontinuous Pd coated semiconducting SWNT were used (4).

Conclusions

In this work, we have presented a detailed analysis of formation of atomic Pd and Pd/Ni chain structures and their interactions with SWNT(6,6) and SWNT(10,0). We found that zigzag chains

are energetically more favorable than linear chains, and the overall binding energy is higher in the Pd/Ni alloy chains than in the pure Pd chains. The addition of Pd and its alloy chains on the tube surface modifies the electronic structure of both types of SWNTs. The chains have similar geometry on the tube surface as in their isolated states, showing stable continuous Pd and Pd/Ni monatomic chains can be formed on SWNTs. The increase of electron density of states around Fermi level enhances the conductivity of SWNT(6,6), whereas the additional states from chains at band gap region effectively transforms SWNT(10,0) into a metal. Charge transfer phenomenon is observed from chain to the tube in all the cases, with a larger amount being transferred from the alloy chain. The Pd/Ni chain also induces a magnetic moment in the tube. We observe that the Pd/Ni narrow angle chain functionalized SWNT(6,6) has much larger magnetic moment than the wide angle chain functionalized SWNT(10,0). Spin density shows the magnetic moment to be mostly concentrated on Ni atoms but on different orbitals determined by the interactions between Pd and Ni in the chains.

Calculations of H_2 interactions with these metal and alloy chain functionalized SWNTs show different degrees of geometrical changes. Due to repulsion between H atoms, the Pd-chain-SWNT(6,6) shows the largest expansion. Our results show that Ni can improve the stability of Pd chain on tube surface, as well as increase the hydrogen adsorption energy. The electronic property calculations indicate a decrease of electron density of states at Fermi level in the functionalized SWNT(6,6), and band gap reopening in the functionalized SWNT(10,0) which turns a metallized (10,0) tube back to semiconductor. These electronic property changes can significantly reduce the conductance of the tubes, which explains the reported experimental observation on Pd functionalized SWNTs in hydrogen sensor applications. We found that both continuous and discrete Pd coating is able to metallize semiconducting SWNT. Although binding energy per Pd atom in the axial functionalized SWNT is same as the radial functionalized, the Pd-C is expected to have a stronger binding in the latter system due to the shorter Pd-C distances. The dramatic decrease of electrical conductance upon H2 adsorptions. The radial chain-functionalized SWNT has a higher hydrogen adsorption energy than axial chain-functionalized SWNT, as well as a less structural relaxation under exposure of H_2.

References

1. Sun, C. Q., Wang, Y., Tay, B. K., Li, S., Huang, H., and Zhang, Y. B. *Journal of Physical Chemistry B* **106**(41), 10701 –10705 (2002).

2. Xie, R. H., Zhao, J., and Rao, Q. *Encyclopedia of nanoscience and nanotechnology* **2**(31), 505–535 (2004).

3. Ciraci, S., Dag, S., Yildirim, T., Gulseren, O., and Senger, R. T. *Journal of Physics-Condensed Matter* **16**(29), R901–R960 (2004).

4. Kong, J., Chapline, M. G., and Dai, H. J. *Advanced Materials* **13**(18), 1384–1386 (2001).

5. Sippel-Oakley, J., Wang, H. T., Kang, B. S., Wu, Z. C., Ren, F., Rinzler, A. G., and Pearton, S. J. *Nanotechnology* **16**(10), 2218–2221 (2005).

6. Lu, Y. J., Li, J., Han, J., Ng, H. T., Binder, C., Partridge, C., and Meyyappan, M. *Chemical Physics Letters* **391**(4-6), 344–348 (2004).

7. Durgun, E., Dag, S., Bagci, V. M. K., Gulseren, O., Yildirim, T., and Ciraci, S. *Physical Review B* **67**(20), 201401 (2003).

8. Durgun, E., Dag, S., Ciraci, S., and Gulseren, O. *Journal of Physical Chemistry B* **108**(2), 575–582 (2004).

9. Yang, C. K., Zhao, J. J., and Lu, J. P. *Physical Review B* **66**(4), 041403 (2002).

10. Bagci, V. M. K., Gulseren, O., Yildirim, T., Gedik, Z., and Ciraci, S. *Physical Review B* **66**(4), 045409 (2002).

11. Singh, D. J. *Planewaves, pseudopotentials, and the LAPW method.* Kluwer Academic Publishers, Boston, (1994).

12. Payne, M. C., Teter, M. P., Allan, D. C., Arias, T. A., and Joannopoulos, J. D. *Reviews of Modern Physics* **64**(4), 1045–1097 (1992).

13. Lee, E. C., Kim, Y. S., Jin, Y. G., and Chang, K. J. *Physical Review B* **66**(7), 073415 (2002).

14. Peng, S. and Cho, K. J. *Nano Letters* **3**(4), 513–517 (2003).

15. Dag, S., Ozturk, Y., Ciraci, S., and Yildirim, T. *Physical Review B* **72**(15), 155404 (2005).

16. Christofides, C. and Mandelis, A. *Journal of Applied Physics* **68**(6), R1–R30 (1990).

17. Favier, F., Walter, E. C., Zach, M. P., Benter, T., and Penner, R. M. *Science* **293**(5538), 2227–2231 (2001).

18. Jakubik, W. P., Urbanczyk, M. W., Kochowski, S., and Bodzenta, J. *Sensors and Actuators B-Chemical* **96**(1-2), 321–328 (2003).

19. Smit, R. H. M., Untiedt, C., Yanson, A. I., and van Ruitenbeek, J. M. *Physical Review Letters* **87**(26), 266102 (2001).

20. Ohnishi, H., Kondo, Y., and Takayanagi, K. *Nature* **395**(6704), 780–783 (1998).

21. Yanson, A. I., Bollinger, G. R., van den Brom, H. E., Agrait, N., and van Ruitenbeek, J. M. *Nature* **395**(6704), 783–785 (1998).

22. Sen, P., Ciraci, S., Buldum, A., and Batra, I. P. *Physical Review B* **64**(19), 195420 (2001).

23. Sanchez-Portal, D., Artacho, E., Junquera, J., Ordejon, P., Garcia, A., and Soler, J. M. *Physical Review Letters* **83**(19), 3884–3887 (1999).

24. Bahn, S. R. and Jacobsen, K. W. *Physical Review Letters* **87**(26), 266101 (2001).

25. Geng, W. T. and Kim, K. S. *Physical Review B* **67**(23), 233403 (2003).

26. Nilius, N., Wallis, T. M., and Ho, W. *Journal of Physical Chemistry B* **108**(38), 14616–14619 (2004).

27. Zhang, Y., Franklin, N. W., Chen, R. J., and Dai, H. J. *Chemical Physics Letters* **331**(1), 35–41 (2000).

28. Marinas, J. M., Campelo, J. M., and Luna, D. *Studies in Surface Science and Catalysis* **27**, 411–457 (1986).

29. Hughes, R. C., Schubert, W. T., and Buss, R. J. *Journal of the Electrochemical Society* **142**(1), 249–254 (1995).

30. Thomas, R. C. and Hughes, R. C. *Journal of the Electrochemical Society* **144**(9), 3245–3249 (1997).

31. Kresse, G. and Hafner, J. *Physical Review B* **47**(1), 558–561 (1993).

32. Kresse, G. and Hafner, J. *Physical Review B* **49**(20), 14251 (1994).

33. Kresse, G. and Furthmuller, J. *Computational Materials Science* **6**(1), 15–50 (1996).

34. Kresse, G. and Furthmuller, J. *Physical Review B* **54**(16), 11169–11186 (1996).

35. Perdew, J. P., Chevary, J. A., Vosko, S. H., Jackson, K. A., Pederson, M. R., Singh, D. J., and Fiolhais, C. *Physical Review B* **46**(11), 6671–6687 (1992).

36. Vanderbilt, D. *Physical Review B* **41**(11), 7892–7895 (1990).

37. Raybaud, P., Kresse, G., Hafner, J., and Toulhoat, H. *Journal of Physics-Condensed Matter* **9**(50), 11085–11106 (1997).

38. Monkhorst, H. J. and Pack, J. D. *Physical Review B* **13**, 5188–5192 (1976).

39. Yagi, Y., Briere, T. M., Sluiter, M. H. F., Kumar, V., Farajian, A. A., and Kawazoe, Y. *Physical Review B* **69**(7), 075414 (2004).

40. Miao, L., Bhethanabotla, V. R., and Joseph, B. (in progress 2006).

41. Reich, S., Thomsen, C., and Ordejon, P. *Physical Review B* **65**(15), 155411 (2002).

42. Gulseren, O., Yildirim, T., and Ciraci, S. *Physical Review B* **65**(15), 153405 (2002).

43. Henkelman, G., Arnaldsson, A., and Jonsson, H. *Computatioinal Materials Science* **36**, 254–360 (2006).

44. Zhao, J. J., Buldum, A., Han, J., and Lu, J. P. *Nanotechnology* **13**(2), 195–200 (2002).

45. Tada, K., Furuya, S., and Watanabe, K. *Physical Review B* **63**(15), 155405 (2001).

46. Dillon, A. C., Jones, K. M., Bekkedahl, T. A., Kiang, C. H., Bethune, D. S., and Heben, M. J. *Nature* **386**(6623), 377–379 (1997).

47. Ahn, C. C., Ye, Y., Ratnakumar, B. V., Witham, C., Bowman, R. C., and Fultz, B. *Applied Physics Letters* **73**(23), 3378–3380 (1998).

48. Kong, J., Franklin, N. R., Zhou, C. W., Chapline, M. G., Peng, S., Cho, K. J., and Dai, H. J. *Science* **287**(5453), 622–625 (2000).

49. Modi, A., Koratkar, N., Lass, E., Wei, B. Q., and Ajayan, P. M. *Nature* **424**(6945), 171–174 (2003).

50. Han, S. S. and Lee, H. M. *Carbon* **42**(11), 2169–2177 (2004).

51. Balasubramanian, K., Feng, P. Y., and Liao, M. Z. *Journal of Chemical Physics* **88**(11), 6955–6961 (1988).

52. Conrad, H., Ertl, G., and Latta, E. E. *surface science* **41**, 435–446 (1974).

53. Wilke, S., Hennig, D., and Lober, R. *Physical Review B* **50**(4), 2548–2560 (1994).

54. Behm, R. J., Christmann, K., and Ertl, G. *Surface Science* **99**(2), 320–340 (1980).

55. Nowick, A. S. and Burton, J. J. *Diffusion in solids.* Academic Press, New York, (1975).

56. Christmann, K., Schober, O., Ertl, G., and Neumann, M. *The journal of chemical physics* **60**(11), 4528–4540 (1973).

57. Madix, R. J., Ertl, G., and Christmann, K. *Chemical Physics Letters* **62**(1), 38–41 (1979).

58. Landolt, M. and Campagna, M. *Physical Review Letters* **39**(9), 568–570 (1977).

59. Muscat, J. P. and Newns, D. M. *Physical Review Letters* **43**(27), 2025–2028 (1979).

60. Peng, S. and Cho, K. *Journal of Applied Mechanics-Transactions of the Asme* **69**(4), 451–453 (2002).

61. Sampedro, B., Crespo, P., Hernando, A., Litran, R., Lopez, J. C. S., Cartes, C. L., Fernandez, A., Ramirez, J., Calbet, J. G., and Vallet, M. *Physical Review Letters* **91**(23), 237203 (2003).

62. Alefeld, G. and Vlkl, J. *Hydrogen in metals.* Topics in applied physics; v. 28-29. Springer-Verlag, Berlin; New York, (1978).

63. Schlapbach, L. and Burger, J. P. *Journal De Physique Lettres* **43**(8), L273–L276 (1982).

64. Bennett, P. A. and Fuggle, J. C. *Physical Review B* **26**(11), 6030–6039 (1982).

65. Chan, C. T. and Louie, S. G. *Physical Review B* **27**(6), 3325–3337 (1983).